Biosensors and Bioelectronics 208 (2022) 114231

Contents lists available at ScienceDirect

Biosensors and Bioelectronics

journal homepage: www.elsevier.com/locate/bios

Aptamer based probes for living cell intracellular molecules detection

Xiaoqin Liu [a], Ting Wang [b], Yuwei Wu [b], Yifu Tan [a], Ting Jiang [a], Ke Li [b], Beibei Lou [b], Liwei Chen [a], Yanfei Liu [a,**], Zhenbao Liu [b,c,*]

[a] Department of Pharmaceutical Engineering, College of Chemistry and Chemical Engineering, Central South University, Changsha, 410083, Hunan Province, PR China
[b] Department of Pharmaceutics, Xiangya School of Pharmaceutical Sciences, Central South University, Changsha, 410013, Hunan Province, PR China
[c] Molecular Imaging Research Center of Central South University, Changsha, 410008, Hunan, PR China

ARTICLE INFO

Keywords:
Aptamer
Biosensor
Intracellular molecule
Fluorescence detection

ABSTRACT

Biosensors have been employed for monitoring and imaging biological events and molecules. Sensitive detection of different biomolecules *in vivo* can reflect the changes of physiological conditions in real-time, which is of great significance for the diagnosis and treatment of diseases. The detection of intracellular molecules concentration change can indicate the occurrence and development of disease. But the analysis process of the existing detection methods, such as Western blot detection of intracellular protein, polymerase chain reaction (PCR) technique quantitative analysis of intracellular RNA and DNA, usually need to extract the cell lysis which is complex and time-consuming. Fluorescence bioimaging enables *in situ* monitoring of intracellular molecules in living cells. By combining the specificity of aptamer for intracellular molecules binding, and biocompatibility of fluorescent materials and nanomaterials, biosensors with different nanostructures have been developed to enter into living cells for analysis. This review summarizes the fluorescence detection methods based on aptamer for intracellular molecules detection. The principles, limit of detection, advantages, and disadvantages of different platforms for intracellular molecular fluorescent response are summarized and reviewed. Finally, the current challenges and future developments were discussed and proposed.

1. Introduction

Monitoring and imaging of biology events and molecules have great significance to the development of biological science. The molecular levels of biomarkers in the body fluid, tissues, and cells can be used to reflect the physical condition of the body, and diagnose or predict diseases (Ghorbani et al., 2019). For example, cytochrome *c* (Cyt *c*) release from mitochondria is a specific event in apoptotic signaling. Assays for intracellular Cyt *c* are needed for apoptosis research (Chen et al., 2015a). However, the detection of Cyt *c in vitro* is usually complex and time-consuming, which contain cell extracts and immunohistochemistry in immobilized cells (Gorbenko et al., 2009; Uren et al., 2005). Biosensors with specific quantitative detection of biological molecules in living cells are urgently needed. The high sensitivity and rapid *in situ* bioimaging strategy can efficiently and real-time monitor the target molecules.

Compared with magnetic resonance imaging and computed tomography, the fluorescence bioimaging method has lower construction costs and higher spatial resolution (Pichler et al., 2010; Qiang et al., 2015). Fluorescence spectroscopic techniques with non-destructive and real-time signaling are used to measure intracellular molecules. The organic dyes, fluorescent nanomaterials, and fluorescent proteins have been developed for biosensors applications (Citartan et al., 2012). When the fluorophores are conjugated with recognition elements, such as antibody and aptamer (Seok Kim et al., 2016), the target molecules can be detected and imaged in living cells and tissues. The aptamer is a single strand of ribonucleic acid (RNA) or deoxyribonucleic acid (DNA) that is selected from the systematic evolution of ligands by exponential enrichment (SELEX) (Ellington and Szostak, 1990; Tuerk and Gold, 1990). The aptamer has many advantages including high selectivity, small size, easily modified, and affinity to various targets such as small molecules, proteins, cells, and tissues, with low dissociation constants.

* Corresponding author. Department of Pharmaceutics, Xiangya School of Pharmaceutical Sciences, Central South University, Changsha, 410013, Hunan Province, PR China.
** Corresponding author. Department of Pharmaceutical Engineering, College of Chemistry and Chemical Engineering, Central South University, Changsha, 410083, Hunan Province, PR China.
E-mail addresses: liuyf@csu.edu.cn (Y. Liu), zhenbaoliu@csu.edu.cn (Z. Liu).

https://doi.org/10.1016/j.bios.2022.114231
Received 23 September 2021; Received in revised form 24 March 2022; Accepted 26 March 2022
Available online 30 March 2022

The selected aptamers can fold into distinct secondary or tertiary structures to interact with molecules.

Aptamer nucleic acid modified with fluorophore can be used as a fluorescence probe to realize intracellular molecule detection. Some nanomaterials with strong optical adsorption capability are ideal nanocarriers and fluorescence quenchers. The quenching groups or nanomaterials can regulate the fluorescence signal of aptamer nanosensor (aptasensor). The dye-labeled aptamers are attached to the nanomaterial via chemisorption, π-π stacking, carboxyl-nucleobase hydrogen bonding, and *van der Waals* forces (He et al., 2020). When aptamer is bind with target molecules, it can recover or quench the fluorescence signal. The fluorescence molecular quenching methods are mostly based on Förster resonance energy transfer (FRET) when a fluorophore is close to a quencher (Crisalli and Kool, 2011). In this paper, we summarize aptamer-based fluorescent probes for intracellular molecules detection. The target-responsive structure changing can lead to the fluorescence signal output. The applications of aptasensor in living cells were comprehensive reviewed (Table 1).

2. Aptamer conjugated with nanomaterials

2.1. Polymer nanoparticles

As a mimic of mussel adhesive proteins, polydopamine (PDAN) can form an adjustable adhesion layer of thickness on any substrate surface or make it into nanospheres for application in biosensors (Cheng et al., 2019). The π-π stacking interaction between nucleobases of aptamer and aromatic groups of PDANs could assembly the aptamer-PDANs complex. The FAM-labeled adenosine triphosphate (ATP)-aptamer (ATP-apt)/PDANs complex had been used for intracellular ATP imaging (Fig. 1A) (Qiang et al., 2015). The abnormal intracellular ATP concentration usually represents changes in cellular metabolism (Dong and Zhao, 2016). The aptamer-PDANs could be delivered into living cells for the quantitative detection of ATP.

Ca^{2+}-doped polydopamine-modified 2D black phosphorus nanosheets (BP@PDA) realized intracellular proteins detection *in vitro* and *in vivo* by conjugation with aptamer (Fig. 1B) (Jiang et al., 2020). The PDA coating overcame the innate instability of BP. When the PDANs were doped with metal ions (e.g., Ca^{2+}, Mg^{2+}), they had a specific affinity with dye-labeled ssDNA via metal coordination between Ca^{2+} and DNA phosphate backbone (Meng et al., 2018), which was conducive to resist displacement, thereby avoid false signals.

Table 1
Intracellular molecules fluorescence detection based on aptamer and nanomaterials.

Nanocarriers	Delivery methods	Target types	Fluorophores	LOD	Refs
PDA	Endocytosis	ATP	FAM	10 μM	Qiang et al. (2015)
GO	Endocytosis	ATP	TPdye	0.5 μM	Yi et al. (2014)
		Cyt *c*	FAM	10 nM	Chen et al. (2015a)
		VEGF165	FAM	0.3 nM	Xu et al. (2019)
		Ochratoxin	FAM	10.4 nM	Xia et al. (2020)
TMDCs	Endocytosis	ATP	Ce6	5 μM	Jia et al. (2015)
		ATP	AgNCs	0.18 nM	Xu et al. (2020)
		IFN-γ	FAM	57.5 pM	Dhenadhayalan et al. (2018)
MXene	Endocytosis	ATP	ROX	0.2 μM	Chu et al. (2021)
MOFs	Endocytosis	ATP	AuNPs	23 nM	Qu et al. (2018)
		ATP	TAMRA/FAM	500 pM	Wang et al. (2017)
		ATP	FAM	8.19 nM	Hai et al. (2018)
		ATP	FAM	4.24 μM	Shi et al. (2021)
Gold nanostructures	Clathrin-mediated endocytosis/Microtubule-dependent transport to lysosomes	ATP	Cy3	200 μM	Wu et al. (2020)
		PLN	Cy5	181 nM	Zhan et al. (2019)
		Glucose	TAMRA	33 nM	Tang et al. (2017)
		Cyt *c*	Cy5	20 nM	Zhang et al. (2019a)
		K^+	Cy3/Texas-Red	4 mM	Cui et al. (2020)
QDs	Endocytosis	Zn^{2+}	FAM	1.54 μM	Shu et al. (2019)
		IFN-γ	GQDs	0.12 pM	Liu et al. (2017a)
UCNPs	Endocytosis	ATP	–	–	Zhao et al. (2018)
		Cyt-c	Cy3	20 nM	Ma et al. (2017)
AIEgen	Endocytosis	IFN-γ	TPEN3	0.6 pM	Ma et al. (2018)
MSNs	Phagocytosis	ATP	FAM	60 nM	Ji et al. (2017)
		ATP	FAM	0.08 nM	Li et al. (2021)
Light-up aptamer	Endocytosis	miRNA	SR-DN	0.3 nM	Ying et al. (2017a)
		SAM	DFHBI	–	Li et al. (2020a)
		EGFR	DIR/OTB	–	Tan et al. (2017)
DNA nanostructures	Caveolin-mediated pathway	ATP (DNA TDN)	TAMRA	10.4 μM	Xie et al. (2016)
		ATP (DNA TP)	Cy3/Cy5	30 μM	Zheng et al. (2017)
		ATP (Hairpin probe)	Alex488	–	Duan et al. (2021)
		ATP (HCR)	Cy3/Cy5	4 μM	Luo et al. (2021)
		ATP (DNA TSP)	–	1 mM	Wang et al. (2020a)

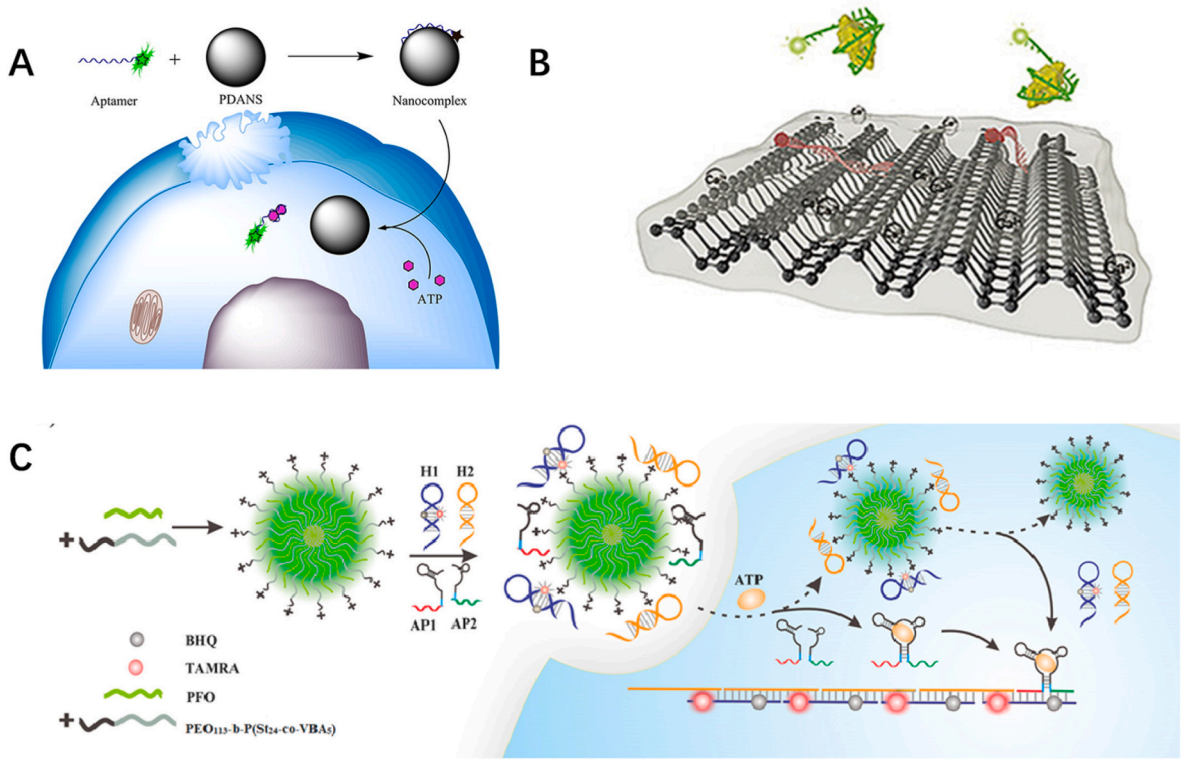

Fig. 1. Interaction polydopamine with dye-labeled aptamer. (A) FAM-labeled ATP-apt/PDANs complex. Copyright 2015, American Chemical Society (Qiang et al., 2015). (B) Ca^{2+}-doped BP@PDA adsorbed with FAM-labeled aptamer. Copyright 2020, Elsevier (Jiang et al., 2020). (C) ATP split aptamer sensor and HCR hairpin probes delivered by BCNs in living cells. Copyright 2018, American Chemical Society (Zhang et al., 2018).

Block copolymer nanoparticles (BCNs) have superior mechanical and physical properties (Blanazs et al., 2009), which consist of two different types of polymers. Due to the positive charge of BCNs, DNA-BCNs complexes could efficiently deliver into cells. Zhang reported an enzyme-free amplification assay for small molecules intracellular detection (Fig. 1C) (Zhang et al., 2018). Two split aptamer fragment probes as recognition elements for ATP and two hybridization chain reaction (HCR) hairpin probes as signal amplifiers were attached on the BCNs via electrostatic and π-π stacking interaction between DNA and BCNs. For *in vitro* ATP detection, the LOD was 30 nM, which is lower than aptamer probes based on PDANS.

2.2. Two-dimensional (2D) nanomaterials

Graphene oxide (GO) and graphene-like nanomaterials, including transition metal dichalcogenides (TMDCs) nanomaterials, transition metal carbide/nitride ($M_{n+1}X_nT_x$, MXene), and metal-organic framework (MOF) are 2D nanomaterials and have broad application prospects for aptamer biosensors with specific surface area and aspect ratio, unique structure (Chimene et al., 2015; Su et al., 2019; Babu et al., 2019). The dye-labeled aptamer probes can be adsorbed on 2D nanomaterials by π-π stacking binding force or *van der Waals* force.

2.2.1. Graphene oxide

GO nano-systems have attracted great attention in biosensing, due to their easy to use and low cost. GO exhibits ultrahigh quenching efficiency and provides large plan surfaces as aptamer nanocarrier for *in situ* monitoring intracellular molecules (Wang et al., 2010; Liu et al., 2014a). The covalent modification of aptamer was reported for ATP detection that is resistant to proteins' nonspecific displacement and DNase I degradation (Fig. 2A) (Liu et al., 2014b). Due to the lower background variation of the covalent ATP aptasensor, the LOD was 0.019 mM which is lower than 0.028 mM of noncovalent aptasensor (Wang et al., 2010). The conformation-resolved (cres) aptamer avoids interference and eliminates the signal fluctuation from other molecules (Ma et al., 2019). Cres-aptamer probes had been developed for monitoring and imaging ochratoxin (OTA) in HeLa cells (Xia et al., 2020). This design strategy had dual recognition mechanism and significantly improved the signal-to-background ratio.

The fluorescent probe can be designed as dual or multiple signal response systems. The FAM-labeled ATP-apt and Cy5-labeled GTP-apt were attached onto GO for ATP and GTP intracellular monitoring (Wang et al., 2014). For multiple signal response systems, four fluorescent aptamer nanoprobes were attached on GO for detection and imaging of tumor-associated proteins in living cells (Xu et al., 2019). This method could simultaneously image four different proteins in the same cell, which could effectively identify cancer cells and normal cells.

However, the shorter excitation wavelengths of one-photon excited (OPE)-dyes produce larger self-absorption, autofluorescence, and photodamages, such as FAM and Cy5. To overcome the limitations, Yi reported two-photon dye (TPdye) labeled aptamer/GO conjugates for ATP imaging by two-photon microscopy (Yi et al., 2014). The TPdye exhibits strong fluorescence emission and anti-Stokes shift under near-infrared (NIR) excitation. TPdye as a signal reporter enhanced the tissue penetration depth, thus improved the performance of sensors in cells and zebrafish.

The fluorescence aptasensor can be designed for visualization targets translocation in living cells. Chen reported a GO/aptasensor for fluorescence activation imaging of Cyt *c* intracellular translocation (Chen et al., 2015a). When the aptamer interacted with Cyt *c*, the aptamer dissociated from GO surface, thus activating fluorescence response, which realized real-time Cyt *c* monitoring in the apoptosis process.

2.2.2. Transition metal dichalcogenides nanomaterials

2D TMDCs materials, such as MoS_2, ReS_2, and TiS_2, are composed of hexagonal planes of positively charged transition metal atoms

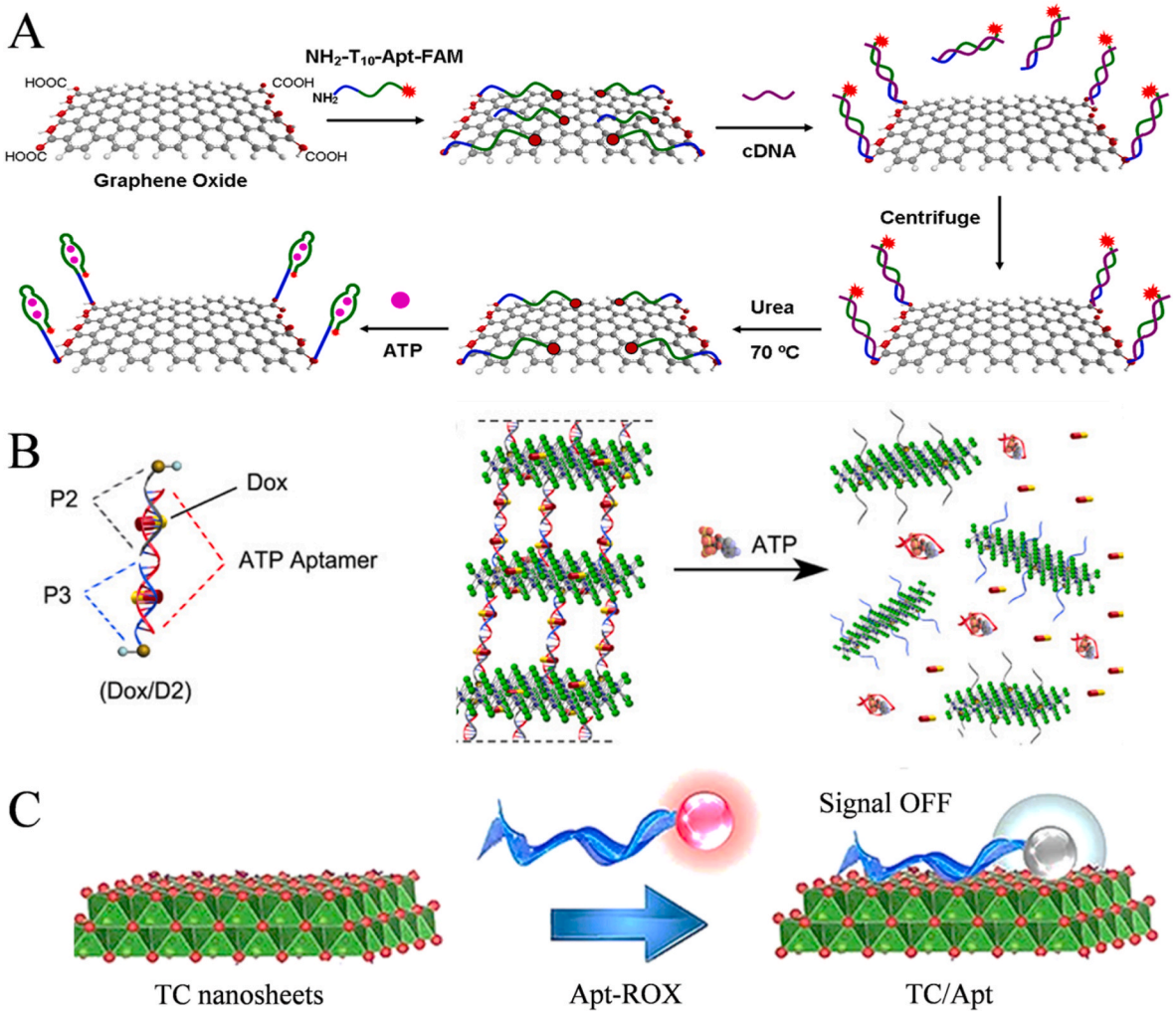

Fig. 2. Interaction 2D nanomaterials with fluorophore/dye-labeled aptamer. (A) The FAM-labeled ATP-apt were covalently attached on GO for ATP imaging. Copyright 2014, American Chemical Society (Liu et al., 2014b). (B) Multilayer MoS_2 nanosheets correlate with ATP-apt and Dox. Copyright 2017, American Chemical Society (Li et al., 2017). (C) A TC nanoprobe to ATP detection by absorbed ROX-tagged aptamer. Copyright 2021, Springer (Chu et al., 2021).

sandwiched between two negatively charged sulfur planes (Coleman et al., 2011). The strong light absorption and fast electron transfer rate make TMDCs nanosheets become fluorescence quenchers for constructing FRET-based detection assay (Babu et al., 2019; Mo et al., 2017).

Due to suitable bandgap, the overall sensitivity of MoS_2-based nanodevices is larger than GO-based nanodevices. The MoS_2 nanosheets also have a strong affinity to aptamer via *van der Waals* force (Zhu et al., 2013). The labeled-aptamer and target could form a rigid conformation that mitigates *van der Waals* force and activates the fluorescence signal (Ge et al., 2014). Jia et al. used a chlorine e6 labeled ATP-apt absorbed on the MoS_2 nanosheets for ATP fluorescence imaging and photodynamic therapy (PDT) (Jia et al., 2015). The multilayer MoS_2 nanosheets were utilized for autonomous ATP-responsive doxorubicin (DOX, cancer therapy drug) delivery (Fig. 2B) (Li et al., 2017).

The MoS_2-lipoic acid-polyethyleneimine (PEI) nanocomposite loaded with ATP-apt fluorescent chain and the quenching chain could achieve ATP metabolism monitoring in glioblastoma stem cells. When nanocomposite triggered by glutathione, the disulfide bond of PEI was cleaved and released the DNA probe (Li et al., 2018). Folic acid was conjugated with MoS_2 nanosheets via chemistry, which can facilitate MoS_2 probe (FA@MoS_2) cellular entry efficiency (Oudeng et al., 2018; Liu et al., 2014c). In Xu's study of ATP intracellular detection (Xu et al., 2020), the ATP-apt was synthesized with silver nanoclusters (AgNCs) loaded on FA@MoS_2. AgNCs acted as a fluoresence label in living cells and an element tag for quantitative analysis in vitro. After cell lysis and removal of the excess probes, ICP-MS was used to quantify intracellular ATP by detecting ^{107}Ag.

Namasivayam compared the ability of ReS_2 and TiS_2 nanosheets combined with FAM-labeled aptamer for detection of intracellular interferon-gamma (IFN-γ) (Dhenadhayalan et al., 2018). The detection limit of IFN-γ using ReS_2 and TiS_2 was evaluated to be 57.6 pM and 82.7 pM, respectively. Accordingly, the ReS_2 nanoprobe showed a higher extent of fluorescence recovery than the TiS_2 nanoprobe in KEK cells.

2.2.3. *Mxene family nanomaterials*

Mxene is a class of 2D materials made from transition metal carbides and carbonitrides with light-to-heat conversion ability and electrical conductivity (Naguib et al., 2011). Mxenes can adsorb nucleic acids by ion bridges and quench the fluorescence dye-labeled DNA (Manzanares-Palenzuela et al., 2019). The titanium carbide (Ti_3C_2) is the most studied Mxenes material for electrochemical or fluorescence biosensors (Deshmukh et al., 2020). Chu et al. presented a 2D titanium carbide nanoprobe for ATP detection by absorbed rhodamine X (ROX)-tagged aptamer in living cells and tumor tissues (Fig. 2C) (Chu et al., 2021). The fluorescence quenching efficiency against ROX of titanium carbide (~97%) was higher than GO (~90%).

2.2.4. Metal-organic frameworks nanomaterials

MOFs are porous materials assembled from metal ions and bridging ligands. The metal and ligand units of MOF can generate luminescence or load guest molecules that can emit or induce luminescence (Deng et al., 2017). MOFs' biodegradability and structural tailorability make them become attractive nanocarriers in virus detection and bioimaging, which were described in detail in our previous paper (Wang et al., 2020b). The 2D MOFs have excellent quenching efficiency for dye-labeled aptamer, reduced the background fluorescence, and improved signal-to-noise (Yang et al., 2019).

MOF-lanthanide-based (MOF-Ln) sensor, with a unique porous structure and large surface area, has preferable sensitivity for ATP recognition (Hao et al., 2019). Wang et al. analyzed living cells' ATP activity by using a two-color nanoprobe that loaded on the MOF-Ln nanosheet by *van der Waals* force (Wang et al., 2017). After incubated with MOF-Ln nanoprobe for 2 or 4 h, the ATP concentration of cells was monitored from 0.5 to 15 nM. The stable 2D H_2dtoaCu MOF nanosheets delocalized the electron system and quenched the fluorescence of FAM-aptamer through a photoinduced electron transfer process (Hai et al., 2018). 2D Cu-MOF conjugated with FAM-labeled ATP-apt nanoprobe was developed for ATP imaging in HeLa cells (Shi et al., 2021). The LOD of Cu-MOF/aptamer for monitoring ATP was tested to be 4.24 μM.

2.3. Metallic nanoparticles

MNPs exhibit nanometal surface energy transfer (NSET), which is a non-radiative energy transfer between metal surface excited states and Fermi levels (Persson and Lang, 1982). The NSET enables more effective fluorescence absorption over a longer distance than that of FRET. There are many advantages of MNPs for being applied in optical biosensors, such as discrete electronic transitions and strong fluorescence (Xu, 2010).

The physical and optical properties of gold nanomaterials with different shapes are different (Table 2). Gold nanostructures (AuNS) are excellent energy acceptors for molecular fluorescence detection and imaging due to their selective functionalization, colloidal stability, and high extinction coefficient. Aptamer modified with sulfur hydrogen bond or polyadenine (poly-A) can be chemically immobilized onto gold nanoparticles (AuNP) surface (Fig. 3A) (Wu et al., 2020; Chen et al., 2017a). The apt@AuNP complexes enter cells through clathrin-mediated endocytosis or transport to lysosomes through microtubule-dependent mechanisms.

Table 2
Different shapes of gold nanomaterials and aptamer nanoplatforms.

Types	Targets	Properties	Refs
Gold nanoparticles	ATP	Controllable size;	Fu et al. (2016)
	PLN	Versatile surface chemistry;	Zhan et al. (2019)
	Glucose	Inherent biologically inert	Tang et al. (2017)
Gold nanoclusters	ATP	Wide variety of feasible synthesis methods; Biocompatibility; High photostability and stability	Lyu et al. (2019)
Gold nanorods	ATP	Amplifying the fluorescence signal; Remoting controlled local heating effect; Simply the ease of surface function;	Guo et al. (2016)
Gold nanocrosses	ATP	Strong plasmonic fields. Large specific surface areas; Excellent tenability; Biocompatibility	Zhang et al. (2019b)
Gold nanotriangles	Cyt *c*	Wide plasma resonance (visible-NIR region); Raman enhancement; Carrier for entering cells	Zhang et al. (2019a)
Gold nanoshells	K^+	Property of photothermal; Efficient broad-spectrum quencher	Cui et al. (2020)

Lyu et al. studied the properties of metal-crosslinked DNA micelles and constructed gold-crosslinked DNA micelles combined with ATP-apt (Fig. 3B) (Lyu et al., 2019). The gold nanoclusters were able to self-deliver into cells by hydrophobic interaction between the lipid residue and hydrophobic membrane. Chen used poly A-based ATP-apt nano-beacons that attached to AuNP for ATP detection (Chen et al., 2017b). They changed the length of polyA anchored on the AuNP surface to improve the detection limit of intracellular ATP. Guo et al. assembled a platform to capture and detect ATP by immobilizing ATP-apt and aptamer against Ramos cell on the surface of gold nanorods (Guo et al., 2016). ATP-apt bound with ATP to release DOX, which was inserted to the double strand DNA of ATP-apt and its complementary DNA. The fluorescence enhancement of DOX could reflect the concentration of ATP.

For intracellular ATP quantitative analysis, the circular dichroism (CD) was employed by fabricating chiral AuNPs-plasmon-mediated heterodimers that assembled DNA zipper-like nanostructures (Fu et al., 2016). The dimers were also labeled with Cy5 for fluorescence confocal location imaging of dimer entry into cytoplasm. The CD intensity induced by ATP showed a linear relationship with the intracellular ATP concentration (linear range: 15–4.2 mM; LOD: 0.2 mM). Zhang et al. designed graphene quantum dots (GQDs) "OFF-ON" switches that are covalently conjugated with ATP-apt and FA for intracellular ATP detection (Zhang et al., 2019b). The LOD was 0.27 mM which was close to the actual intracellular ATP levels.

Zhan et al. synthesized a fluorescence nanoprobe and specifically detected intracellular phospholamban (PLN) micro-peptide by applying AuNPs and Cy5-labeled aptamer that connected with thiol-modified short cytosine-strand (Zhan et al., 2019). The nanoprobe directly entered cardiomyocytes through endocytosis because the AuNPs became the oligonucleotides' shell which enhanced probe stability and cellular uptake. They realized qualitative and quantitative detection of PLN in living cardiomyocytes and mice heart frozen tissue sections using this nanoprobe.

Liposomes are mimics cell membranes that have been used as delivery carriers for drugs and nucleotides. Tang used liposomes that contained Shinkai's receptor and aptamer to detect intracellular glucose under different oxygen concentrations (Tang et al., 2017). When this nano-system entered into HeLa cells, Shinkai's receptor bound with glucose to form a complex, then the aptamer recognized the Shinkai-glucose complex, and the fluorescence was restored.

Zhang et al. assembled Cyt *c* aptamer and Cy5-labeled complementary strand into gold nanotriangles (AuNTs) that obtained surface-enhanced Raman scattering (SERS)-fluorescence double-mode biosensors for the quantitative detection of Cyt *c* (Fig. 3C) (Zhang et al., 2019a). The AuNTs acted as carriers, Raman-enhancing substrate, and quenching agents. The Raman or fluorescence signal showed linear relationships with the concentration of Cyt *c*.

Photothermal gold nanoshells and aminated silica nanoparticles core were used as nanocarriers for "lock" the dual-strand potassium ions (K^+) aptamer precursor (DSAP) (Cui et al., 2020). After NIR irradiation, the local temperature of AuNS was increased for de-hybridizing, dissociating and releasing K^+ aptamer for K^+ detection. The Cy3 and Texas-Red (donor and acceptor) were labeled at two ends of the aptamer, and the FRET signal could be turn-on during the detection process. The LOD reached 4 mM.

AgNCs are nanocarriers and luminescent indicators for building fluorescence aptamer probes. The DNA-AgNCs fluorescence probe shows strong binding ability, low toxicity, and good biocompatibility (Ritchie et al., 2007). 8-hydroxydeoxyguanosine (8-OHdG) aptamer containing 12 cytosines were conjugated with AgNCs (8-OHdG-12-C@AgNCs) for intracellular 8-OHdG imaging (Lan et al., 2020). 8-OHdG

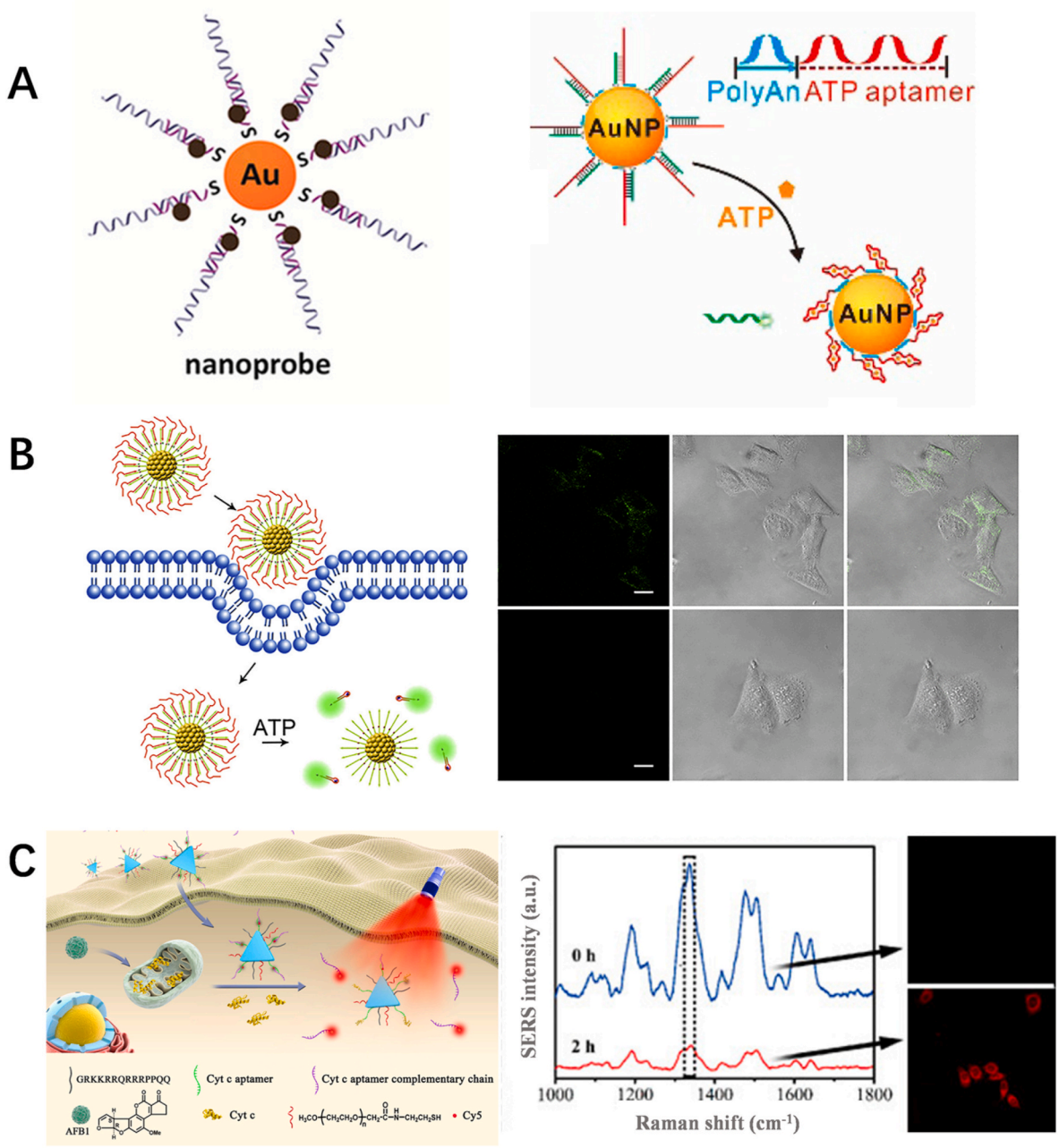

Fig. 3. Interaction gold nanomaterials with aptamer for fluorescence monitor. (A) Aptamer modified with sulfur hydrogen bond or polyadenine chemically immobilized or attached onto AuNPs' surface. Copyright 2017, American Chemical Society. Copyright 2019, American Chemical Society (Zhan et al., 2019; Chen et al., 2017a). (B) Gold-crosslinked DNA micelles combined with ATP-apt for ATP imaging in HeLa cells. Copyright 2019, Elsevier (Lyu et al., 2019). (C) Cyt c-apt assembled into AuNTs for the SERS quantitative assay of Cyt *c*. Copyright 2019, American Chemical Society (Zhang et al., 2019a). (For interpretation of the references to color in this figure legend, the reader is referred to the Web version of this article.)

was the main product during DNA oxidative stress injury. The levels of oxidative stress injury were positively correlated with the aggregation of 8-OHdG-12C@AgNCs in cells and the detection range was 0–100 μM.

2.4. Quantum dots

Quantum dots (QDs) are used as superior fluorophores and the donors or acceptors of FRET in biosensors, due to the strong photoluminescence and photostability, unique size-dependent optical properties, and the broad absorption and narrow emission spectra (tailored from the NIR to UV) (Hildebrandt et al., 2017). The aptamer-QDs nanoprobe, combined with teicoplanin-AuNPs (the FRET acceptor), was used for *Staphylococcus aureus* detection in Raw 264.7 cells (Fig. 4A) (Fu et al., 2020). Photosensitizers TMPyP-Zn-QD and quencher (BHQ_2)-labeled ATP-apt were used for imaging-guided cancer therapy (Shen et al., 2017). When the ATP-apt bind with ATP, the aptamer released from QDs and then triggered photodynamic therapy in HeLa tumors. Carbon dot (CD) showed a long half-life in cell interior and exhibited excellent performance for intracellular metal detection. Shu et al. reported a FAM-labeled Zn^{2+}-aptamer that modified with CDs for intracellular Zn^{2+} imaging and quantification in living cells (Shu et al., 2019). The ICP/MS was used to quantify the CDs content to obtain the linear relationship between fluorescence ratio ($(F–F_0)/F_0$, $F=I_{CDs}/I_{FAM}$) and zinc content. Linear calibration of 34.7–60.3 fg/cell was obtained in MCF-7 cells. GQDs were applicated for IFN-γ label-free detection in living cells by aggregation-disaggregation sensing strategy (Fig. 4B) (Liu

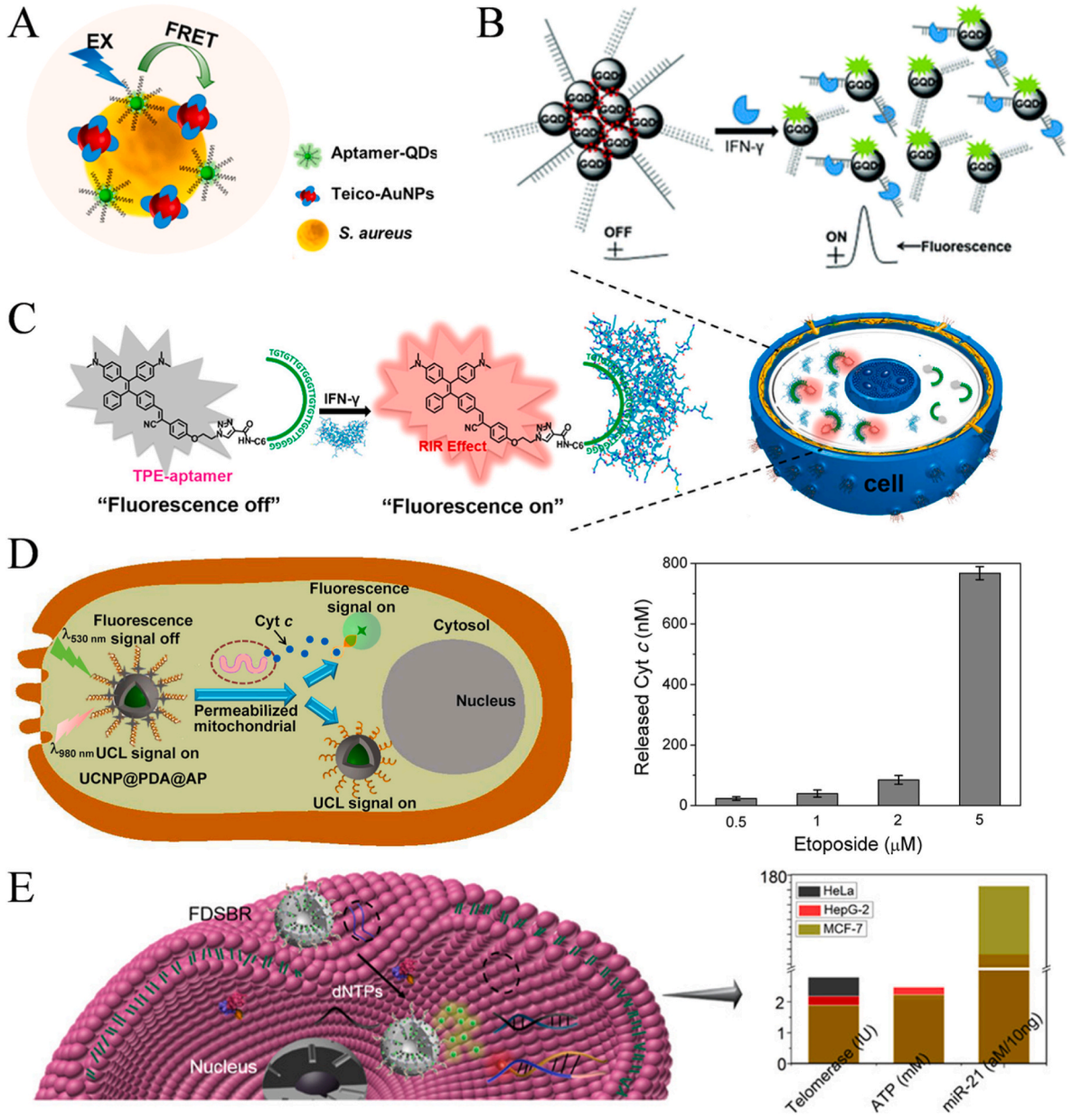

Fig. 4. Nanomaterials modified with aptamer for fluorescence monitor. (A) Aptamer-QDs combined teicoplanin-AuNPs nanoprobe for *Staphylococcus aureus* detection. Copyright 2020, American Chemical Society (Fu et al., 2020). (B) GQDs applicated for detection of IFN-γ in living cells. Copyright 2017, Royal Society of Chemistry (Liu et al., 2017a). (C) TPEN3 and IFN-γ aptamer for IFN-γ detection. Copyright 2018, American Chemical Society (Ma et al., 2018). (D) UCNPs-core@shell structure coated with PDA and aptamer for Cyt *c* detection. Copyright 2016, Elsevier (Ma et al., 2017). (E) Detection and quantitative analysis of molecular multi-targets based on MSNs. Copyright 2020, American Chemical Society (Huang et al., 2020).

et al., 2017a). In the presence of IFN-γ, the Apt-GQDs and Epitope-GQDs would disaggregate to turn on the fluorescent, and vice versa.

2.5. Aggregation-induced emission fluorogen (AIEgen)

The AIEgen-based aptasensor is a label-free probe with no background interference and owns switch-on emission property. When the complexation between aptamer and targets is formed, AIE-based aptamer probes can restrict intramolecular rotations, resulting in strong emission of fluorescence (Ma et al., 2018; Hong et al., 2011). Ma used an AIEgen-based aptasensor that consisted of TPEN3 (AIEgen) and IFN-γ aptamer for IFN-γ detection in BV2 cell (Fig. 4C) (Ma et al., 2018). TPE-aptamer fluorescence emission was induced by IFN-γ. The LOD of TPE-aptamer was determined to be 0.6 pM, which is lower than the aptamer sensor based on TMDCs (Dhenadhayalan et al., 2018).

2.6. Upconversion nanoparticles

Rare-earth (RE) ions doped upconversion nanoparticles (UCNPs) exhibit excellent photostability (nor photo-blinking and photobleaching) and low excitation energy in NIR. UCNPs can emit high-energy luminescence under low-energy excitation because their electronic structure has the anti-stokes shift. Hence, UCNPs can minimize the luminescence from uninterest molecules to improve the signal-to-noise ratio (Jin et al., 2017). UCNPs have photo-conversion ability to absorb NIR light and emit UV or NIR light locally. When UCNPs are combined with photolysis (photocleavable) materials, the NIR region-activated DNA probe with deep-tissue-penetrability can be realized. Zhao integrated lanthanide-doped UCNPs and ATP-apt using a photocleavable (PC) group linker (Zhao et al., 2018). The Apt-Act/UCNPs were incubated with HeLa cells or injected into HeLa

tumor-bearing mice, followed by 980 nm NIR irradiation for 2 h, the PC dissociated from ATP-apt and resulted in a dramatic increase in the fluorescent signal.

A UCNPs-core@shell structure was coated with polydopamine to provide an active surface and quench the fluorescence of Cy3-labeled Cyt *c*-aptamer (Fig. 4D) (Ma et al., 2017). The steady upconversion luminescent signal was employed for intracellular imaging. And the most important, the ratio of UCNP's intensity and the increased fluorescence intensity of Cy3 ($F_R = \Delta F_{cy3}/F_{ucnp660}$) demonstrated a linear correlation with Cyt *c* concentration.

2.7. Silica nanoparticles

Mesoporous silica nanoparticles (MSNs) are applicable delivery vehicles in biosensors and drug delivery systems. The MSNs have high surface area, uniform cylindrical structure, tunable nanoscale size, and functionable surface (Asefa and Tao, 2012). They also offer a "reservoir" for storing some "cargoes" (e.g., fluorescein, nucleotides, or drugs), and their opening and closing can be controlled. The AuNPs modified with ATP-apt blocked the core of MSNs, and the aptamers were hybridized with the ssDNA which was attached to MSNs via NH_2-groups. After completing the target binging event, the AuNPs got away from the surface of MSNs to release FAM (LOD was 60 nM) (Ji et al., 2017). A MSN platform with ATP responsive drugs release was also designed (Zheng et al., 2015). GQDs absorbed the ATP-apt via π-π stacking interaction can be used to cap the pores and quench the fluorescence. In the presence of ATP, ATP-apt bound with ATP and GQDs was released, thus the synchronized ATP detection and DOX release were realized.

Huang synthesized universal probes for molecular multi-targets detection and quantitative analysis based on amine-modified and double-strand DNA (dsDNA) labeled MSNs (Fig. 4E) (Huang et al., 2020). By changing the composition of dsDNA, the concentrations of telomerase, ATP, miR-21 were quantified in different cells. This probe had a potential application for cell screening due to it could reflect different levels of multi-biomarkers in different cell lines.

TPdye-doped silica nanoparticles (energy donor) and amino-modified hairpin primers with FAM (energy acceptor) were designed as a signal-off nanoprobe for ATP imaging in MCF-7 cells and liver tissues (Li et al., 2021). Fluorophores and two-photon SiNPs were separated by hybridization of aptamer with hairpin primers. ATP concentration correlated with fluorescence intensity ratio in the range of 0–5.0 mM and the LOD was tested to be 0.08 nM.

3. Signaling RNA aptamer nanoplatforms

Light-up RNA aptamers (fluorogenic aptamers) can specifically turn on or enhance fluorescence upon binding with a condition fluorophore which exhibits low fluorescence when free in biological mediums (Swetha et al., 2020). The stable secondary structure of light-up RNA aptamer is inherently resistant to nuclease degradation while is challenging to interact with cellular components. By fusing a target-responsive sensing element (sensing aptamer unit) and a light-up aptamer (working aptamer unit) through a junction region (e.g., tRNA scaffold), a new fluorescence signaling RNA aptamer had been constructed (Ying et al., 2017a). Some other fluorescence signaling RNA aptamers for detection of intracellular molecules are summarized in Table 3. The structure of light-up aptamer is controlled by a sensing domain. During the target combination, the structure of light-up aptamer recovers, and makes them restore the binding ability to the fluorophore.

3.1. Signaling RNA aptamer nanoplatforms for miRNA imaging

For living cell RNA imaging, the strategy of signal-responsive is similar to classic molecular beacon and fluorescence *in situ* hybridization (Su and Hammond, 2020). The sensing domain is a complementary sequence of target RNA. MicroRNA (miRNA) imaging and localized spatial distribution in living Hun7 and HEK293T cells were realized by changing the structure of Spinach (modSpinach) (Fig. 5A) (Ying et al., 2017b). A structurally interacting RNA switch was utilized for miRNA binding. When the FASTmiR sensor was "turn-on", the modSpinach exhibited strong fluorescence upon binding with DFHBI (3,5-difluoro-4-hydroxybenzylidene imidazolinone). The DFHBI-binding RNA aptamers (Spinach and Broccoli) could split into two complementary fragments, each containing a partially specific recognition segment of mRNA (Fig. 5B) (Wang et al., 2018). When mRNA hybridized with split-aptamer in human cells, the two fragments changed spatial proximity and formed a fluorophore-binding site. The spatial distance between target RNA sequences has potential applications for *in vivo* visualization of RNA-RNA interaction. The light irradiation can induce the cis-trans isomerization of DFHBI (Wang et al., 2013). The transform of DFHBI subsequently unbound with the aptamer resulting in the fluorescence intensity decrease. A derivative of DFHBI called benzimidazole (BI) substituent was generated for markedly increased brightness and photostability (Li et al., 2020a). The BI fluorophore had faster-ejected speed upon the isomerization to trans form. A broccoli array that binds with BI for single mRNA imaging in live cells was developed.

Jiang used a stem-loop-shaped miRNA responsive motif that incorporated with sulforhodamine B (SR)-binding aptamer and engineered a recombinant tRNA (Fig. 5C) (Ying et al., 2017a). When miRNA was hybridized with its complementary loop, the SR-binding loop would fold spotaneously for conjugating SR-dinitroaniline (DN) fluorophore-quencher pairs that followed an enhanced fluorescence signal (red). By co-expression of the RNA sensor with green fluorescence (GFP), dual-emission ratiometric imaging was realized. The ratio of red-green fluorescence intensity was dynamically correlated with the concentration of miRNA-21 in living cells. But, the two separate promoters might affect expression efficiency.

Signal amplification strategy for RNA aptamer detecting miRNA had been studied to solve the under-expressed of miRNA in single cells. For example, rolling circle transcription synchronization machinery (RCTsm) of "turn-on" RNA aptamer strategy for let-7a miRNA detection (Fig. 5D) (Li et al., 2020c). In this method, the LOD was calculated to be 6.1 fM *in vitro*. Another signal amplification strategy without any additional enzymes was described by a Twister-optimized RNA for a durable overexpression system (Litke and Jaffrey, 2019).

3.2. Signaling RNA aptamer nanoplatforms for SAM imaging

Spinach and Broccoli are green fluorescent fluorogenic aptamers. These probes suffer from the green background fluorescence of

Table 3
Fluorescence signaling RNA aptamers for detection of intracellular molecules.

Targets	Working region	Sensing aptamers	Junction region	Fluorophores	Refs
miRNA-21	Complementary loop	SR-binding aptamer	tRNA	SR-DN	Ying et al. (2019)
miRNA-122	sxRNA	Spinach	Three-way junction	DFHBI	Ying et al. (2017b)
SAM	SAM aptamer	Broccoli	Transducer	DFHBI-1T	Li et al. (2020b)
SAM	SAM aptamer	Broccoli	Transducer	OBI	Li et al. (2020a)
EGFR	Anti EGFR aptamer	DIR2s	Transducer	DIR/OTB	Tan et al. (2017)

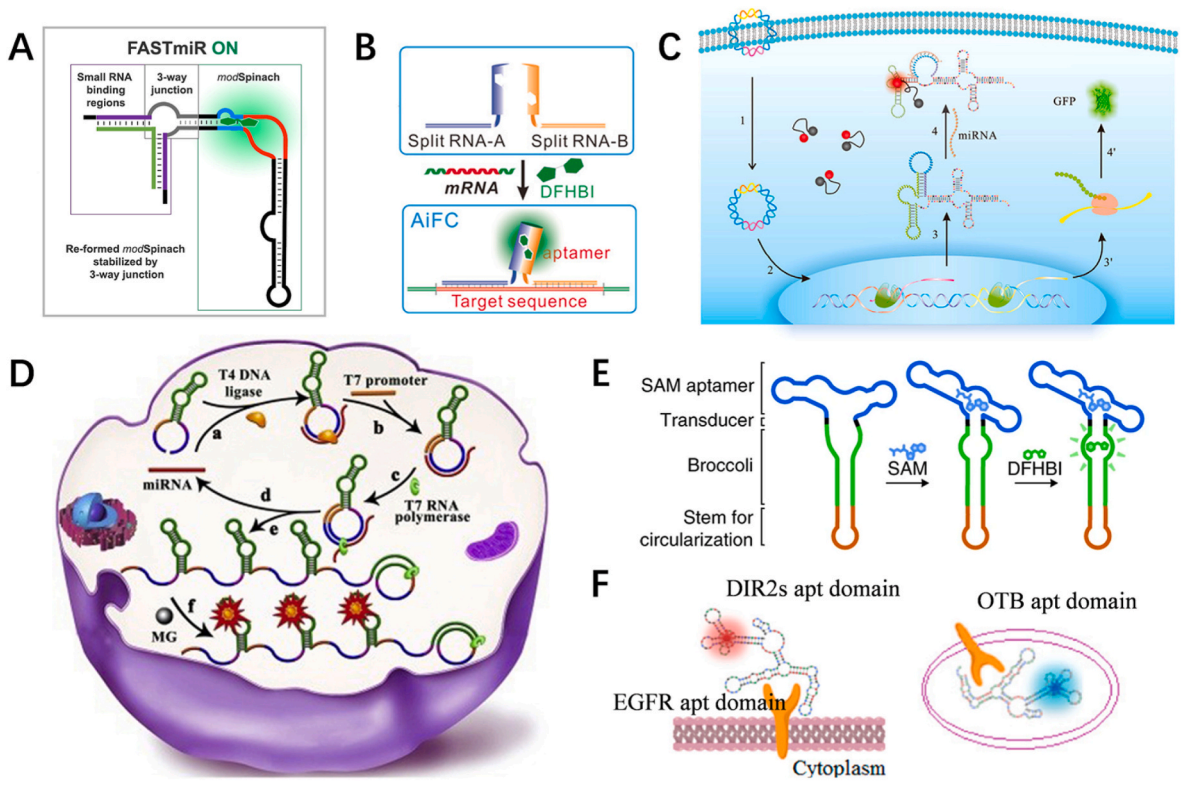

Fig. 5. Signaling RNA aptamer nanoplatforms detected intracellular molecules. (A) The FASTmiR sensor contain a sxRNA switch at ON-state. Copyright 2017, Oxford academic (Ying et al., 2017b). (B) DFHBI-binding RNA aptamers split into two complementary fragments each contains a partially specific recognition segment of mRNA. Copyright 2017, Angewandte Chemie (Wang et al., 2018). (C) A stem-loop-shaped miRNA responsive motif that incorporation with SR-binding aptamer and engineered a recombinant tRNA. Copyright 2017, American Chemical Society (Ying et al., 2017a). (D) RCTsm of "turn-on" RNA aptamer strategy for let-7a miRNA detection. Copyright 2020, Elsevier (Li et al., 2020c). (E) The SAM aptamer was fused into the racRNA for cellular metabolites imaging. Copyright 2019, Nature (Litke and Jaffrey, 2019). (F) The DIR2s-Apt fused to 3′-terminus of anti-EGFR RNA aptamer to distinguish between cell-surface and internalized EGFR. Copyright 2017, American Chemical Society (Tan et al., 2017).

endogenous cellular flavins and nicotinamide adenine dinucleotide. Some groups focused on designing broccoli binding to red fluorophore, such as 3,5-difluoro-4-hydroxybenzylidene imidazolinone-2-oxime (DFHO) (Song et al., 2017). Li prepared a new fluorophore, 3,5-difluoro-4-hydroxybenzylidene imidazolinone-2-oxime-1 benzoimidazole (OBI), that combined red broccoli with high affinity and photostability (Li et al., 2020a). The metabolite S-adenosyl methionine (SAM)-binding aptamer was fused with red broccoli by a transducer domain. After being treated with the SAM inhibitor, the brightness of cells was noticeably reduced.

The nanomolar concentration of the light-up RNA aptamer in mammalian cells prevents the use of signaling aptamer. A rapid RNA circularization device with high stability and expression levels had been described (Fig. 5E) (Litke and Jaffrey, 2019). A twister-optimized RNA for durable overexpression (Tornado) system was used to obtain the stale circular RNA aptamer of interest in mammalian cells that reached micromolar concentration. The twister ribozymes in the tornado transcripts underwent autocatalytic cleavage. The ubiquitous endogenous RNA ligase had ligated the leaving termini that formed a racRNA (ribozyme-assisted circular RNA). The SAM aptamer was fused into the racRNA for cellular metabolites imaging.

3.3. Signaling RNA aptamer nanoplatforms for protein imaging

A new RNA fluorogenic aptamer that allows dual-fluorescent labeling has been studied. Armitage reported an aptamer that the DIR2s-Apt could specifically activate the fluorescence of dimethylindole red (DIR) and oxazole thiazole blue (OTB) (Fig. 5F) (Tan et al., 2017). In live-cell imaging, they fused the DIR2s-Apt to 3′-terminus of anti-epidermal growth factor receptor (EGFR) RNA aptamer to distinguish between cell-surface and internalized EGFR. The EGFR-DIR2s aptamer and OTB were incubated with A431 cells at 37 °C for 30 min for detection of intracellular EGFR. After washing the external fusion aptamer and dye, the cells were incubated with EGFR-DIR2s aptamer and DIR on ice for cell-surface EGFR imaging. This dual-labeled aptamer provides a novel method for studying the internalization of cell receptors.

4. DNA nanoplatforms

DNA molecules can fabricate nano-architectures for different sizes and shapes with inherent biocompatibility, sequence programmability, and manipulability (Gao et al., 2020). Framework nucleic acids are self-assembled DNA nanostructures that have the capacity of tailorable functionality and precise program for intracellular molecular detection and biological imaging (Zhou et al., 2021). Suitable size of DNA nanostructures can enter into the cell without extra transfection agents (Liang et al., 2014).

4.1. DNA tetrahedron

Tetrahedron DNA (TDN) is a kind of 3D nanostructure, which consists of four DNA or RNA nucleic acid chain via a thermal annealing process (Goodman et al., 2005). Due to the rigid structure of TDN, it can resist enzymatic degradation and exhibit excellent biocompatibility, and its edges or vertices can provide modification sites for functional ligands (Giovanni et al., 2015; Li et al., 2011; Mitchell et al., 2009). TDNs nanostructures can internalize through a caveolin-mediated pathway and subsequently enter lysosomes or engage intracellular motion to rely

on microtubules (Liang et al., 2014). Peng used two TDNs with branched vertexes that contained a ATP-binding aptamer and an i-motif tethered to vertexes in lysosomes (Fig. 6A) (Peng et al., 2019). The cell lysosome uptaken pathway of TDNs had been verified and achieved TDN nanoplatforms for ATP imaging at the subcellular level.

The structurally variable TDN nanoprobe had been designed for nucleic acid devices for cellular logic computation. The DNA logic-gate system can exhibit programmed configuration switching upon responding to external stimuli. Pei used the dynamic TDNs to demonstrate various scaffolded logic gates (INH, XOR, OR, AND) for fluorescence response of protons, Hg^{2+}, ATP, and complementary DNA strands (Pei et al., 2012). It provides a nanoplatform for multiple targets analysis or design of drug-controlled release systems. In Zhou's study, multilateral modification of TDN was utilized for simultaneous detection of multiplex analytes (Fig. 6B) (Zhou et al., 2020), including three different miRNAs and three different endonucleases. Unlike the above approach that the entire aptamer sequence was integrated into the TDN, the aptamer or oligonucleotide could partially hybridize with half-stem and loop of hairpin structure of TDN edge (Xie et al., 2016). When introduced the target strand, the aptamer was kept away from the

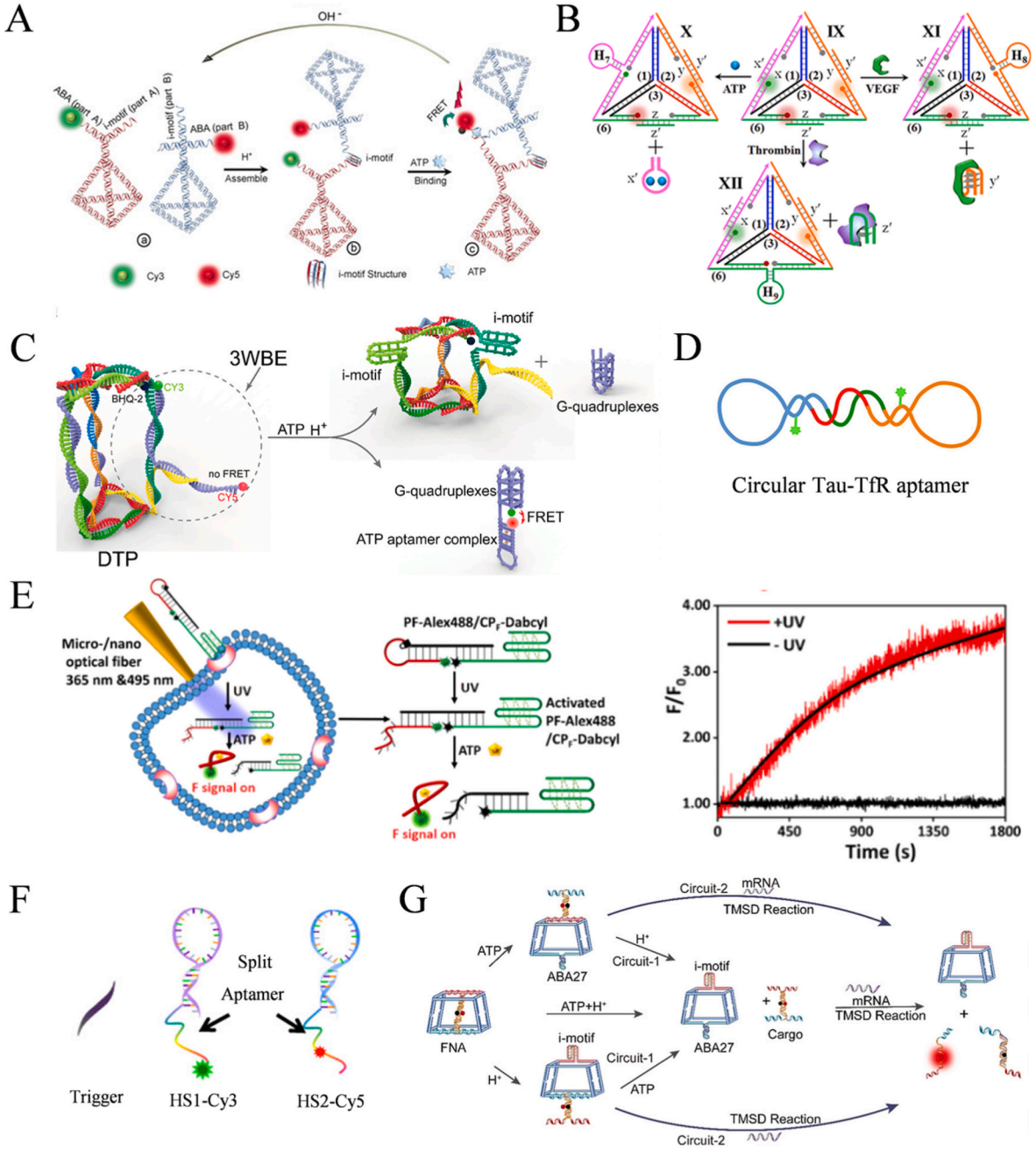

Fig. 6. DNA nanoplatforms containing aptamers for intracellular molecules detection. (A) Two TDNs with branched vertexes that contained ATP-binding aptamer and an i-motif tethered to vertexes in lysosomes. Copyright 2018, Angewandte Chemie (Peng et al., 2019). (B) Multilateral modification of TDN was utilized for simultaneous detection of multiplex analytes. Copyright 2020, American Chemical Society (Zhou et al., 2020). (C) The i-motif and ATP-apt were contained in DNA TP for subcellular imaging. Copyright 2019, American Chemical Society (Du et al., 2019). (D) A cb-aptamer consists of TfR aptamer and Tau aptamer. Copyright 2020, American Chemical Society (Li et al., 2020d). (E) Photo-responsive hairpin DNA nanostructures for ATP imaging (Duan et al., 2021). (F) Hybridization chain reaction and ATP split aptamer for mitochondrial ATP imaging. Copyright 2021, American Chemical Society (Luo et al., 2021). (G) TSP caged with ATP-apt and i-motif for sensing ATP and protons. Copyright 2020, Angewandte Chemie (Wang et al., 2020a).

tetrahedron, then formed a hairpin structure and FRET was turned on. They used this probe for detection and imaging of intracellular ATP with LOD being 10.4 μM.

4.2. DNA triangular prism

DNA triangular prism (TP) is constructed with three long base clip sequences through a module integrating design strategy (Liu et al., 2017b). The DNA TP exhibits good structural rigidity and remarkable cellular penetration. DNA TP nanostructure can provide the hybridization sites for aptamer on unilateral horizontal sides of the top and bottom surfaces. Zheng detected ATP in living cells based on split aptamer and DNA TP (Zheng et al., 2017). In the presence of the target, it can reassemble into binding shape by "induced-fit effect". The split aptamers bond to Cy3 and Cy5, respectively. The detection concentration range of ATP using TP nanosensor was 0.03–5 mM with a LOD of 30 μM *in vitro*. DNA TPs also could be used as framework nucleic acid devices for cellular logic computation (Peng et al., 2018). The i-motif and ATP-binding aptamer were contained in the three-way branched edge of DNA TP for subcellular imaging (Fig. 6C) (Du et al., 2019). When this nanodevice entered lysosomes via caveolae-mediated endocytosis, the abnormal levels of lysosomal pH and ATP could affect logic input via FRET. This nanodevice has the potential application in the lysosomes diseases diagnosis.

4.3. Circular bivalent aptamer

A new modulate aptamer structure strategy is to produce bifunctional circular bivalent aptamer (cb-apt). The cb-apt is covalently linked to the 3′-terminus of an aptamer with the 5′-terminus of either the same or another aptamer, using ligase or complementary hybridization. The cb-apt lacks free ends that can improve thermal and physical stability in biological media compared to linear nucleic acid (Kuai et al., 2017). In both qualitative and quantitative experiments, the specificity and binding affinities of the cb-apt have almost negligible changes with the monofunctional aptamer (Le et al., 2013). The cb-apt also enhanced internalization, accumulation, and retention *in vivo*. Some researchers synthesized a circular aptamer composed of transferrin receptor (TfR) aptamers, which could promote TfR aptamer recognition and induce cell transport across the blood-brain barrier endothelial cells (Fig. 6D) (Chen et al., 2008; Yu et al., 2011). Another monofunctional aptamer of cb-apt was Tau protein aptamer or epithelial cell adhesion molecule aptamer (SYL3C) for diagnostic and therapeutic of brain diseases (Li et al., 2020d; Macdonald et al., 2017).

4.4. Other DNA nanostructures

Hairpin DNA nanoprobes are composed of an oligo-nucleic acid chain containing aptamer sequence and fluorophore/quencher groups, which is the simplest DNA nanostructure. A photo-responsive hairpin DNA nanostructure was composed of Dabcyl-AS1411 and ATP-apt, which was modified with Alex488 and a photocleavable linker (Fig. 6E) (Duan et al., 2021). When the photo-responsive unit was activated by UV irradiation or two-photon, ATP would interact with aptamer in MCF-7 cells and release fluorescence signal of Alex488. This light response mode could effectively avoid the occurrence of false-positive or false-negative signals.

Hybridization chain reaction and ATP split aptamers (HS1-Cy3 and HS2-Cy5) were constructed for mitochondrial ATP imaging (Fig. 6F) (Luo et al., 2021). In this work, the pathway of cellular uptake of fluorescence DNA nanostructures was identified as caveolin-dependent endocytosis. But the different physicochemical properties of fluorescence might affect intracellular distribution of DNA nanostructures. The DNA nanostructures labeled with Cy3 and Cy5 tended to localize to mitochondria, while those labeled with FAM tended to deliver into lysosomes.

DNA-computation circuits based on truncated square pyramid (TSP) nanocarriers were reported (Fig. 6G) (Wang et al., 2020a), which were constructed by four-component strands. The TSP caged with ATP-apt and i-motif that responded to ATP and protons in lysosomes and antisense oligonucleotides containing duplex of TK1 mRNA for downstream mRNA imaging. The LOD of ATP and mRNA based on TSP logic circuits *in vitro* were 1 mM and 1 nM, respectively. OR-AND and AND-AND logic circuits consisting of cascaded gates were tested in different cells that entered cells through caveolin-dependent receptor-mediated endocytosis.

DNA hydrogel with highly three-dimensional networks has the potential to develop biocompatible hydrogel (Lee et al., 2012). Synthetic polymers and pure DNA are typical backbones to preparation DNA hydrogels that have application restrictions in living organisms due to the organic reagents and uncontrolled size of hydrogels (Kahn et al., 2017). Li et al. employed three Y-shaped types of streptavidin-based DNA tetrad to assemble size-controlled and high biocompatibility DNA hydrogels (SDH) (Li et al., 2019). The SDH containing ATP-apt and DOX were used for intracellular ATP imaging and tumor therapy.

5. Summary and conclusion

This review is focused on intracellular molecules detection in living cells based on aptamers and fluorescence bioimaging. To overcome the problems of single nucleic acid aptamer, such as poor cellular internalization and easy to be degraded by nuclease, nanomaterials with different functions were introduced into the construction of aptamer nano-sensors. These nanomaterials are not only used as nanocarriers with high biocompatibility, some even can alter fluorescence signals of the fluorophore. The development of nanomaterials with fluorescence properties (e.g., QDs, MXene, UCNPs) can contribute to label-free aptamer nano-sensors. But the degradation mechanisms and longtime safety of nanomaterials, such as PDA, GO, TMDCs, MOF, AuNPs, QD, are unclear. Furthermore, the weak stability of MXene and MOFs in a physiological environment, particle aggregation of AuNPs and QDs, and the difficult preparation method of MSNs may restrict the using of suitable materials for aptasensing. By comparison, the signaling RNA aptamer nanoplatforms and DNA nanoplatforms are safer and can avoid the complicated steps of preparation. The DNA nanoplatforms can even be designed with precise programmed function. However, the LOD of DNA nanoplatforms for the same molecules (such as ATP) are higher than the nanomaterial platforms (Table 1), indicating the detection sensitivity of DNA nanoplatforms needs to be improved. In general, based on rational and effective design of aptamers, fluorescent materials and nanocarriers, the detection performances can be improved.

The properties of nano-carrier materials determine the detection performances of aptamer fluorescence probes. Firstly, the fluorescence biosensors are affected by the low tissue penetration ability and autofluorescence background. NIR fluorescence imaging method with low toxicity and high controllability of space and time can be partially overcome the above weakness (Yi et al., 2014). However, the ensuing concern is the need of NIR fluorescence imaging equipment. The instability quantum efficiencies of label-free aptamer fluorescence probes reduced their sensitivities for intracellular detection. Secondly, the endocytic mechanisms of aptamer probes are seldom investigated (Yoon and Rossi, 2018). Different endocytosis determines the distribution of aptamer probes into different organelles. The interactions of aptamer probes with endogenous macromolecules usually affect the performance and sensitivity (Chen et al., 2015b). Thirdly, according to the existing aptasensor reports on the quantitative detection of intracellular molecules in living cells, fluorescence quantitative methods (such as ratiometric bioimaging) in living cells couldn't get accurate concentration value when compared with quantitative analysis techniques combined with fluorescence detection (Table 4). Therefore, fluorescence aptasensor strategy for accurate quantitative analysis in cytoplasm is still lacking. Finally, a multifunctional aptasensor is needed to identify cells

Table 4
The intracellular molecules quantitative analysis based on aptamer and fluorescence detection.

Targets	Nanoplatforms	Fluorophores	Quantitative analysis methods	Cells	Linear ranges	Detection limits	Refs
ATP	Gold nanoparticles	Cy5	Circular dichroism	Hela	1.5–4.2 mM	0.2 mM	Fu et al. (2016)
Cyt *c*	Gold nanotriangles	Cy5	Surface-enhanced Raman scattering	HepG2	0.0436–9.95 μM	0.02 μM	Zhang et al. (2019a)
Cyt *c*	UCNP@PDA	Cy3	Upconversion luminescent (UCL) signals	HepG2	50 nM-10 μM	20 nM	Ma et al. (2017)
ATP	Silica nanoparticles	FAM/TPdye (2-naphthalenecarboxylic acid)	Ratiometric bioimaging	MCF-7	–	–	Li et al. (2021)

and diagnose disease by comparing the analytical concentrations of multiple substances (such as logic computation based on DNA nanostructures). Generally, the specific design of nucleic acid sequences and the conformational changes of DNA nanostructures after aptamer binding with targets limit the development of universal probes. However, through optimization of various nanocarriers and fluorescent groups, fluorescence biosensors can reduce LODs and improve sensitivity in the living cells, which has great potential in future real-time intracellular molecule detection applications.

6. Future perspectives

Current research for aptamer fluorescence detection is focused on the performance optimization of recognition elements and fluorescent materials. Modifying the internal structure of the nucleic acid chain can improve the stability of the aptamer probe to reduce the use of some nanomaterials. Conformation-resolved aptamer nanoprobes (cresAptamer) were fabricated for molecule sensing (Xia et al., 2020). The cresAptamer owns a dual recognition mechanism: binding-induced release from nanocarriers and response of intrinsic G-quadruplex of aptamers. The dual recognition resolved the nonspecific binding of aptamer probes. The cresAptamer significantly improves the signal-to-background ratio for sensitively and robustly imaging ochratoxin A in living cells. The signal response system with a simple structure and resistance to degradation will undoubtedly reduce the preparation process and cost. Through rational design of the system, logical responsive or multi-substances responsive system will be realized. The development of automation and intelligent aptamer fluorescent probes for simultaneous detection of multiple targets can be more accurate in the diagnosis of diseases. Molecular quantitative analysis in living cells is also an important development direction of aptasensors. Significantly, a molecular radar strategy based on CRISPR technology was developed to diagnose small molecules (such as ATP) (Niu et al., 2021). The aptamer labeled with fluorophore and quencher at its two ends was used as a ssDNA activator that binds to crRNA-Cas12a, which activated Cas12a and showed trans-cleavage activity. The fluorescence signal intensity was related to the concentration of Cas12a and target. The nano-probe system realizes different intracellular molecules detection by changing types of aptamers contributed to the construction of universal platforms and personalized medicines (Zhang et al., 2019c). According to the physical signs of different patients, different diagnostic proposals will be provided. Intracellular molecular imaging-guided precise therapy of tumors is a new type of theranostics system, which can be reasonably designed for diagnosis and therapy different stages of cancer. Based on aptamer targeted activation of fluorescence, and site specifically drug release, it can greatly improve the treatment effect of cancer.

Declaration of competing interest

The authors declare that they have no known competing financial interests or personal relationships that could have appeared to influence the work reported in this paper.

Acknowledgements

This work was financially supported by the Innovation-Driven Project of Central South University (2020CX048), the National Natural Science Foundation of China (81301258), the Natural Science Foundation of Changsha (kq2202131), the Natural Science Foundation of Hunan Province (2019JJ60071, 2020JJ4680), the Shenghua Yuying Project of Central South University, the Postgraduate Innovation Project of Central South University (2020zzts819, 2020zzts408, 2020zzts409, 2021zzts0977, 2021zzts0979), and the Open-End Fund for the Valuable and Precision Instruments of Central South University.

References

Asefa, T., Tao, Z., 2012. Chem. Res. Toxicol. 25, 2265–2284.
Babu, E., Bhuvaneswari, J., Muthu Mareeswaran, P., Thanasekaran, P., Lee, H.-M., Rajagopal, S., 2019. Coord. Chem. Rev. 380, 519–549.
Blanazs, A., Armes, S.P., Ryan, A.J., 2009. Macromol. Rapid Commun. 30, 267–277.
Chen, C.-h.B., Dellamaggiore, K.R., Ouellette, C.P., Sedano, C.D., Lizadjohry, M., Chernis, G.A., Gonzales, M., Baltasar, F.E., Fan, A.L., Myerowitz, R., Neufeld, E.F., 2008. Proc. Natl. Acad. Sci. Unit. States Am. 105, 15908–15913.
Chen, T.T., Tian, X., Liu, C.L., Ge, J., Chu, X., Li, Y., 2015a. J. Am. Chem. Soc. 137, 982–989.
Chen, Y.-J., Groves, B., Muscat, R.A., Seelig, G., 2015b. Nat. Nanotechnol. 10, 748–760.
Chen, L., Chao, J., Qu, X., Zhang, H., Zhu, D., Su, S., Aldalbahi, A., Wang, L., Pei, H., 2017a. ACS Appl. Mater. Interfaces 9, 8014–8020.
Chen, L.Z., Chao, J., Qu, X.M., Zhang, H.B., Zhu, D., Su, S., Aldalbahi, A., Wang, L.H., Pei, H., 2017b. ACS Appl. Mater. Interfaces 9, 8014–8020.
Cheng, W., Zeng, X., Chen, H., Li, Z., Zeng, W., Mei, L., Zhao, Y., 2019. ACS Nano 13, 8537–8565.
Chimene, D., Alge, D.L., Gaharwar, A.K., 2015. Adv. Mater. 27, 7261–7284.
Chu, B., Wang, A., Cheng, L., Chen, R., Shi, H., Song, B., Dong, F., Wang, H., He, Y., 2021. J. Nanobiotechnol. 19, 187.
Citartan, M., Gopinath, S.C.B., Tominaga, J., Tan, S.-C., Tang, T.-H., 2012. Biosens. Bioelectron. 34, 1–11.
Coleman, J.N., Lotya, M., O'Neill, A., Bergin, S.D., King, P.J., Khan, U., Young, K., Gaucher, A., De, S., Smith, R.J., Shvets, I.V., Arora, S.K., Stanton, G., Kim, H.-Y., Lee, K., Kim, G.T., Duesberg, G.S., Hallam, T., Boland, J.J., Wang, J.J., Donegan, J.F., Grunlan, J.C., Moriarty, G., Shmeliov, A., Nicholls, R.J., Perkins, J.M., Grieveson, E. M., Theuwissen, K., McComb, D.W., Nellist, P.D., Nicolosi, V., 2011. Science 331, 568–571.
Crisalli, P., Kool, E.T., 2011. Bioconjugate Chem. 22, 2345–2354.
Cui, M.-R., Chen, L.-X., Li, X.-L., Xu, J.-J., Chen, H.-Y., 2020. Anal. Chem. 92, 4558–4565.
Deng, J., Wang, K., Wang, M., Yu, P., Mao, L., 2017. J. Am. Chem. Soc. 139, 5877–5882.
Deshmukh, K., Kovářík, T., Khadheer Pasha, S.K., 2020. Coord. Chem. Rev. 424, 213514.
Dhenadhayalan, N., Sriram, M.I., Lin, K.-C., 2018. Sensor. Actuator. B Chem. 258, 929–936.
Dong, J., Zhao, M., 2016. Trac. Trends Anal. Chem. 80, 190–203.
Du, Y., Peng, P., Li, T., 2019. ACS Nano 13, 5778–5784.
Duan, Z., Tan, L., Duan, R., Chen, M., Xia, F., Huang, F., 2021. Anal. Chem. 93, 11547–11556.
Ellington, A.D., Szostak, J.W., 1990. Nature 346, 818–822.
Fu, P., Sun, M., Xu, L., Wu, X., Liu, L., Kuang, H., Song, S., Xu, C., 2016. Nanoscale 8, 15008–15015.
Fu, F., Zhang, Y., Li, L., Wang, H., Li, Q., Tao, X., Song, Y., Song, E., 2020. Anal. Chem. 92, 11462–11468.
Gao, Y., Li, Q., Zhang, J., Wu, C., Shen, Z., Xue, C., Chang, H.T., Wu, Z.S., 2020. ACS Appl. Mater. Interfaces 12, 3341–3353.
Ge, J., Ou, E.C., Yu, R.Q., Chu, X., 2014. J. Mater. Chem. B 2, 625–628.
Ghorbani, F., Abbaszadeh, H., Dolatabadi, J.E.N., Aghebati-Maleki, L., Yousefi, M., 2019. Biosens. Bioelectron. 142, 111484.
Giovanni, M., Setyawati, M.I., Tay, C.Y., Qian, H., Kuan, W.S., Leong, D.T., 2015. Adv. Funct. Mater. 25, 3840–3846.

Goodman, R.P., Schaap, I.A.T., Tardin, C.F., Erben, C.M., Berry, R.M., Schmidt, C.F., Turberfield, A.J., 2005. Science 310, 1661–1665.
Gorbenko, G.P., Trusova, V.M., Molotkovsky, J.G., Kinnunen, P.K.J., 2009. Biochim. Biophys. Acta Biomembr. 1788, 1358–1365.
Guo, Y., Li, S., Liu, J., Yang, G., Sun, Z., Wan, J., 2016. Sensor. Actuator. B Chem. 235, 655–662.
Hai, X.M., Li, N., Wang, K., Zhang, Z.Q., Zhang, J., Dang, F.Q., 2018. Anal. Chim. Acta 998, 60–66.
Hao, Y.B., Shao, Z.S., Cheng, C., Xie, X.Y., Zhang, J., Song, W.J., Wang, H.S., 2019. ACS Appl. Mater. Interfaces 11, 31755–31762.
He, Q., Wu, Q., Feng, X., Liao, Z., Peng, W., Liu, Y., Peng, D., Liu, Z., Mo, M., 2020. Int. J. Biol. Macromol. 151, 757–780.
Hildebrandt, N., Spillmann, C.M., Algar, W.R., Pons, T., Stewart, M.H., Oh, E., Susumu, K., Díaz, S.A., Delehanty, J.B., Medintz, I.L., 2017. Chem. Rev. 117, 536–711.
Hong, Y., Lam, J.W.Y., Tang, B.Z., 2011. Chem. Soc. Rev. 40, 5361–5388.
Huang, S., Zhang, Q., Yao, H., Wang, W., Zhang, J.R., Zhu, J.J., 2020. ACS Sens. 5, 1149–1157.
Ji, X., Lv, H., Zhang, W., Ding, C., 2017. J. Anal. Chem. 72, 437–444.
Jia, L., Ding, L., Tian, J., Bao, L., Hu, Y., Ju, H., Yu, J.S., 2015. Nanoscale 7, 15953–15961.
Jiang, H., Xia, Q., Liu, D., Ling, K., 2020. Anal. Chim. Acta 1121, 1–10.
Jin, B., Wang, S., Lin, M., Jin, Y., Zhang, S., Cui, X., Gong, Y., Li, A., Xu, F., Lu, T.J., 2017. Biosens. Bioelectron. 90, 525–533.
Kahn, J.S., Hu, Y., Willner, I., 2017. Acc. Chem. Res. 50, 680–690.
Kuai, H., Zhao, Z., Mo, L., Liu, H., Hu, X., Fu, T., Zhang, X., Tan, W., 2017. J. Am. Chem. Soc. 139, 9128–9131.
Lan, J., Feng, B., Wu, X., Yang, L., Liu, J., Shi, G., Wang, F., 2020. ACS Appl. Nano Mater. 3, 1332–1338.
Le, T.T., Scott, S., Cass, A.E.G., 2013. Anal. Chim. Acta 761, 143–148.
Lee, J.B., Peng, S., Yang, D., Roh, Y.H., Funabashi, H., Park, N., Rice, E.J., Chen, L., Long, R., Wu, M., Luo, D., 2012. Nat. Nanotechnol. 7, 816–820.
Li, J., Pei, H., Zhu, B., Liang, L., Wei, M., He, Y., Chen, N., Li, D., Huang, Q., Fan, C., 2011. ACS Nano 5, 8783–8789.
Li, B.L., Setyawati, M.I., Chen, L., Xie, J., Ariga, K., Lim, C.T., Garaj, S., Leong, D.T., 2017. ACS Appl. Mater. Interfaces 9, 15286–15296.
Li, N., Zhang, W., Khan, M., Lin, L., Lin, J.M., 2018. Biosens. Bioelectron. 99, 142–149.
Li, N., Wang, X.Y., Xiang, M.H., Liu, J.W., Yu, R.Q., Jiang, J.H., 2019. Anal. Chem. 91, 2610–2614.
Li, X., Mo, L., Litke, J.L., Dey, S.K., Suter, S.R., Jaffrey, S.R., 2020a. J. Am. Chem. Soc. 142, 14117–14124.
Li, X., Kim, H., Litke, J.L., Wu, J., Jaffrey, S.R., 2020b. Angew Chem. Int. Ed. Engl. 59, 4511–4518.
Li, D., Yang, F., Yuan, R., Xiang, Y., 2020c. Anal. Chim. Acta 1102, 84–90.
Li, X., Yang, Y., Zhao, H., Zhu, T., Yang, Z., Xu, H., Fu, Y., Lin, F., Pan, X., Li, L., Cui, C., Hong, M., Yang, L., Wang, K.K., Tan, W., 2020d. J. Am. Chem. Soc. 142, 3862–3872.
Li, D., Liu, Y., Yu, S., Zhang, D., Wang, X., Zhong, H., He, K., Wang, Y., Wu, Y.X., 2021. Analyst 146, 4945–4953.
Liang, L., Li, J., Li, Q., Huang, Q., Shi, J., Yan, H., Fan, C., 2014. Angew. Chem. Int. Ed. 53, 7745–7750.
Litke, J.L., Jaffrey, S.R., 2019. Nat. Biotechnol. 37, 667–675.
Liu, Z., Liu, B., Ding, J., Liu, J., 2014a. Anal. Bioanal. Chem. 406, 6885–6902.
Liu, Z., Chen, S., Liu, B., Wu, J., Zhou, Y., He, L., Ding, J., Liu, J., 2014b. Anal. Chem. 86, 12229–12235.
Liu, T., Wang, C., Gu, X., Gong, H., Cheng, L., Shi, X., Feng, L., Sun, B., Liu, Z., 2014c. Adv. Mater. 26, 3433–3440.
Liu, G., Zhang, K., Ma, K., Care, A., Hutchinson, M.R., Goldys, E.M., 2017a. Nanoscale 9, 4934–4943.
Liu, Y., Chen, Q., Liu, J., Yang, X., Guo, Q., Li, L., Liu, W., Wang, K., 2017b. Anal. Chem. 89, 3590–3596.
Luo, L., Wang, M., Zhou, Y., Xiang, D., Wang, Q., Huang, J., Liu, J., Yang, X., Wang, K., 2021. Anal. Chem. 93, 6715–6722.
Lyu, Y., Guo, Y., Cai, R., Peng, R., Hong, C., Chen, X., Hou, W., Li, X., Tan, J., Zou, Y., Zhang, X., Liu, Q., Tan, W., 2019. Inside Chem. 5, 913–928.
Ma, L., Liu, F., Lei, Z., Wang, Z., 2017. Biosens. Bioelectron. 87, 638–645.
Ma, K., Zhang, F., Sayyadi, N., Chen, W., Anwer, A.G., Care, A., Xu, B., Tian, W., Goldys, E.M., Liu, G., 2018. ACS Sens. 3, 320–326.
Ma, Y., Geng, F., Wang, Y., Xu, M., Shao, C., Qu, P., Zhang, Y., Ye, B., 2019. Biosens. Bioelectron. 134, 36–41.
Macdonald, J., Henri, J., Goodman, L., Xiang, D., Duan, W., Shigdar, S., 2017. ACS Chem. Neurosci. 8, 777–784.
Manzanares-Palenzuela, C.L., Pourrahimi, A.M., Gonzalez-Julian, J., Sofer, Z., Pykal, M., Otyepka, M., Pumera, M., 2019. Chem. Sci. 10, 10010–10017.
Meng, Y., Liu, P., Zhou, W., Ding, J., Liu, J., 2018. ACS Nano 12, 9070–9080.
Mitchell, N., Schlapak, R., Kastner, M., Armitage, D., Chrzanowski, W., Riener, J., Hinterdorfer, P., Ebner, A., Howorka, S., 2009. Angew. Chem. Int. Ed. 48, 525–527.
Mo, L., Li, J., Liu, Q., Qiu, L., Tan, W., 2017. Biosens. Bioelectron. 89, 201–211.
Naguib, M., Kurtoglu, M., Presser, V., Lu, J., Niu, J., Heon, M., Hultman, L., Gogotsi, Y., Barsoum, M.W., 2011. Adv. Mater. 23, 4207.
Niu, C., Wang, C., Li, F., Zheng, X., Xing, X., Zhang, C., 2021. Biosens. Bioelectron. 183, 113196.
Oudeng, G., Au, M., Shi, J., Wen, C., Yang, M., 2018. ACS Appl. Mater. Interfaces 10, 350–360.
Pei, H., Liang, L., Yao, G., Li, J., Huang, Q., Fan, C., 2012. Angew. Chem. Int. Ed. 51, 9020–9024.
Peng, R., Zheng, X., Lyu, Y., Xu, L., Zhang, X., Ke, G., Liu, Q., You, C., Huan, S., Tan, W., 2018. J. Am. Chem. Soc. 140, 9793–9796.
Peng, P., Du, Y., Zheng, J., Wang, H., Li, T., 2019. Angew. Chem. Int. Ed. 58, 1648–1653.
Persson, B.N.J, Lang, N.D, 1982. Phy. Rev. B 26 (10), 5409.
Pichler, B.J., Kolb, A., Nägele, T., Schlemmer, H.-P.J., 2010. Nucl. Med. 51, 333.
Qiang, W., Hu, H., Sun, L., Li, H., Xu, D., 2015. Anal. Chem. 87, 12190–12196.
Qu, F., Sun, C., Lv, X., You, J., 2018. Mikrochim. Acta 185, 359.
Ritchie, C.M., Johnsen, K.R., Kiser, J.R., Antoku, Y., Dickson, R.M., Petty, J.T., 2007. J. Phys. Chem. C Nanomater. Interfaces 111, 175–181.
Seok Kim, Y., Ahmad Raston, N.H., Bock Gu, M., 2016. Biosens. Bioelectron. 76, 2–19.
Shen, Y., Tian, Q., Sun, Y., Xu, J.J., Ye, D., Chen, H.Y., 2017. Anal. Chem. 89, 13610–13617.
Shi, X., Xu, H., Wu, Y., Zhao, Y., Meng, H.-M., Li, Z., Qu, L., 2021. J. Analysis Testing 5, 165–173.
Shu, Y., Zheng, N., Zheng, A.Q., Guo, T.T., Yu, Y.L., Wang, J.H., 2019. Anal. Chem. 91, 4157–4163.
Song, W., Filonov, G.S., Kim, H., Hirsch, M., Li, X., Moon, J.D., Jaffrey, S.R., 2017. Nat. Chem. Biol. 13, 1187–1194.
Su, Y., Hammond, M.C., 2020. Curr. Opin. Biotechnol. 63, 157–166.
Su, S., Sun, Q., Gu, X., Xu, Y., Shen, J., Zhu, D., Chao, J., Fan, C., Wang, L., 2019. Trac. Trends Anal. Chem. 119, 115610.
Swetha, P., Fan, Z., Wang, F., Jiang, J.H., 2020. J. Mater. Chem. B 8, 3382–3392.
Tan, X., Constantin, T.P., Sloane, K.L., Waggoner, A.S., Bruchez, M.P., Armitage, B.A., 2017. J. Am. Chem. Soc. 139, 9001–9009.
Tang, J., Ma, D., Pecic, S., Huang, C., Zheng, J., Li, J., Yang, R., 2017. Anal. Chem. 89, 8319–8327.
Tuerk, C., Gold, L., 1990. Science 249, 505–510.
Uren, R.T., Dewson, G., Bonzon, C., Lithgow, T., Newmeyer, D.D., Kluck, R.M., 2005. J. Biol. Chem. 280, 2266–2274.
Wang, Y., Li, Z., Hu, D., Lin, C.-T., Li, J., Lin, Y., 2010. J. Am. Chem. Soc. 132, 9274–9276.
Wang, P., Querard, J., Maurin, S., Nath, S.S., Le Saux, T., Gautier, A., Jullien, L., 2013. Chem. Sci. 4, 2865–2873.
Wang, Y., Tang, L., Li, Z., Lin, Y., Li, J., 2014. Nat. Protoc. 9, 1944–1955.
Wang, H.-S., Li, J., Li, J.-Y., Wang, K., Ding, Y., Xia, X.-H., 2017. NPG Asia Mater. 9, e354.
Wang, Z., Luo, Y., Xie, X., Hu, X., Song, H., Zhao, Y., Shi, J., Wang, L., Glinsky, G., Chen, N., Lal, R., Fan, C., 2018. Angew. Chem. Int. Ed. 57, 972–976.
Wang, H., Peng, P., Wang, Q., Du, Y., Tian, Z., Li, T., 2020a. Angew Chem. Int. Ed. Engl. 59, 6099–6107.
Wang, Y., Hu, Y.Q., He, Q.Y., Yan, J.H., Xiong, H.J., Wen, N.C., Cai, S.D., Peng, D.M., Liu, Y.F., Liu, Z.B., 2020b. Biosens. Bioelectron. 169, 112604.
Wu, D., Zhao, P., Wu, L., Lin, L., Yu, G., Xu, L., Yue, J., 2020. ACS Appl. Bio Mater. 3, 4590–4599.
Xia, X., Zhang, T., Deng, S., Chen, J., Wu, S., He, C., Zhang, K., Deng, R., He, Q., 2020. ACS Sustain. Chem. Eng. 8, 9920–9925.
Xie, N., Huang, J., Yang, X., Yang, Y., Quan, K., Ou, M., Fang, H., Wang, K., 2016. ACS Sens. 1, 1445–1452.
Xu, H., Suslick, K.S. 22(2010), pp. 1078-1082..
Xu, J.Y., Chen, W.T., Shi, M., Huang, Y., Fang, L.N., Zhao, S.L., Yao, L.F., Liang, H., 2019. Microchim. Acta 186, 204.
Xu, Y., Kang, Q., Yang, B., Chen, B., He, M., Hu, B., 2020. Anal. Chim. Acta 75–83.
Yang, Q., Hong, J., Wu, Y.-X., Cao, Y., Wu, D., Hu, F., Gan, N., 2019. ACS Appl. Mater. Interfaces 11, 41506–41515.
Yi, M., Yang, S., Peng, Z., Liu, C., Li, J., Zhong, W., Yang, R., Tan, W., 2014. Anal. Chem. 86, 3548–3554.
Ying, Z.M., Wu, Z., Tu, B., Tan, W., Jiang, J.H., 2017a. J. Am. Chem. Soc. 139, 9779–9782.
Ying, Z.-M., Wu, Z., Tu, B., Tan, W., Jiang, J.-H., 2017b. J. Am. Chem. Soc. 139, 9779–9782.
Ying, Z.M., Yuan, Y.Y., Tu, B., Tang, L.J., Yu, R.Q., Jiang, J.H., 2019. Chem. Sci. 10, 4828–4833.
Yoon, S., Rossi, J.J., 2018. Adv. Drug Deliv. Rev. 134, 22–35.
Yu, Y.J., Zhang, Y., Kenrick, M., Hoyte, K., Luk, W., Lu, Y., Atwal, J., Elliott, J.M., Prabhu, S., Watts, R.J., Dennis, M.S., 2011. Sci. Transl. Med. 3, 84ra44.
Zhan, R., Li, X., Guo, W., Liu, X., Liu, Z., Xu, K., Tang, B., 2019. ACS Sens. 4, 733–739.
Zhang, C.-H., Wang, H., Liu, J.-W., Sheng, Y.-Y., Chen, J., Zhang, P., Jiang, J.-H., 2018. ACS Sens. 3, 2526–2531.
Zhang, J., Ma, X., Wang, Z., 2019a. Anal. Chem. 91, 6600–6607.
Zhang, R.Y., Sun, J.D., Ji, J., Pi, F.W., Xiao, Y., Zhang, Y.Z., Sun, X.L., 2019b. Sensor. Actuator. B Chem. 282, 910–916.
Zhang, J., Cui, Y.-X., Feng, X.-N., Cheng, M., Tang, A.-N., Kong, D.-M., 2019c. ACS Appl. Mater. Interfaces 11, 39624–39632.
Zhao, J., Gao, J., Xue, W., Di, Z., Xing, H., Lu, Y., Li, L., 2018. J. Am. Chem. Soc. 140, 578–581.
Zheng, F.F., Zhang, P.H., Xi, Y., Chen, J.J., Li, L.L., Zhu, J.J., 2015. Anal. Chem. 87, 11739–11745.
Zheng, X., Peng, R., Jiang, X., Wang, Y., Xu, S., Ke, G., Fu, T., Liu, Q., Huan, S., Zhang, X., 2017. Anal. Chem. 89, 10941–10947.
Zhou, Z., Sohn, Y.S., Nechushtai, R., Willner, I., 2020. ACS Nano 14, 9021–9031.
Zhou, Y., Zhuo, Y., Peng, R., Zhang, Y., Du, Y., Zhang, Q., Sun, Y., Qiu, L., 2021. Sci. China Chem. 64, 1817–1825.
Zhu, C., Zeng, Z., Li, H., Li, F., Fan, C., Zhang, H., 2013. J. Am. Chem. Soc. 135, 5998–6001.